HHS Public Access

Author manuscript

ACS Appl Mater Interfaces. Author manuscript; available in PMC 2019 April 08.

Published in final edited form as:

ACS Appl Mater Interfaces. 2018 October 24; 10(42): 35830–35837. doi:10.1021/acsami.8b14534.

Temperature-Controlled Reversible Exposure and Hiding of Antimicrobial Peptides on an Implant for Killing Bacteria at Room Temperature and Improving Biocompatibility in Vivo

Jiezhao Zhan[#†], **Lin Wang**[#†], **Yuchen Zhu**[†], **Huichang Gao**[‡], **Yunhua Chen**[†], **Junjian Chen**[†], **Yongguang Jia**[‡], **Jingcai He**[†], **Zhou Fang**[†], **Ye Zhu**[§], **Chuanbin Mao**[*,§], **Li Ren**[*,‡], and **Yingjun Wang**[*,†]

[†] School of Materials Science and Engineering, South China University of Technology, Guangzhou 510641, China

[‡] National Engineering Research Center for Tissue Restoration and Reconstruction, Guangzhou 510006, China

[§] Department of Chemistry and Biochemistry, Stephenson Life Sciences Research Center, Institute for Biomedical Engineering, Science and Technology, University of Oklahoma, Norman, Oklahoma 73019, United States

[#] These authors contributed equally to this work.

Abstract

Modification of implants by antimicrobial peptides (AMPs) can improve the antimicrobial activity of the implants. However, AMPs have some cytotoxicity in vivo when they are exposed at body temperature. To tackle this challenge, we propose to develop a new approach to generating a smart antimicrobial surface through exposure of AMPs on the surface. A polydopamine film was first formed on the substrates, followed by the conjugation of a temperature-sensitive polymer, (*N*-isopropylacrylamide) (pNIPAM), to the film through atom transfer radical polymerization (ATRP). Then, AMPs were conjugated to the NIPAM on the resultant pNIPAM-modified surface through a click chemistry reaction. Because of the temperature-sensitive property of pNIPAM, the AMPs motif was more exposed to the external environment at room temperature (25 °C) than at body temperature (37 °C), making the surface present a higher antimicrobial activity at room temperature than at body temperature. More importantly, such a smart behavior is accompanied with the increased biocompatibility of the surface at body temperature when compared to the substrates unmodified or modified by AMPs or pNIPAM alone. Our in vivo study further verified that pNIPAM-AMP dual modified bone implants showed increased biocompatibility even when

[*]Corresponding Authors: cbmao@ou.edu (C.M.), psliren@scut.edu.cn (L.R.), imwangyj@scut.edu.cn (Y.W.).

ASSOCIATED CONTENT

Supporting Information

The Supporting Information is available free of charge on the ACS Publications website at DOI: 10.1021/acsami.8b14534.

Evaluation ofthe N1s high-resolution spectra ofeach step, the surface mass density of grafted AMP, and the MIC of AMPs, the Br 3d (a) and Cu 2p (b) high-resolution spectra of Ti-pNIPAM-AMP, and LIVE/DEAD image of different surfaces after incubation against *E. coli* for 2 h at 37 and 25 °C, and the biocompatibility of AMPs (PDF)

Notes

The authors declare no competing financial interest.

they were challenged with the bacteria at room temperature before implantation. These results indicate that the implants are antibacterial at room temperature and can be safely employed during surgery, resulting in no infection after implantations. Our work represents a new promising strategy to fully explore the antimicrobial property of AMPs, while improving their biocompatibility in vivo. The higher exposure of AMPs at room temperature (the temperature for storing the implants before surgery) will help decrease the risk of bacterial infection, and the lower exposure of AMPs at body temperature (the temperature after the implants are placed into the body by surgery) will improve the biocompatibility of AMPs.

Graphical Abstract

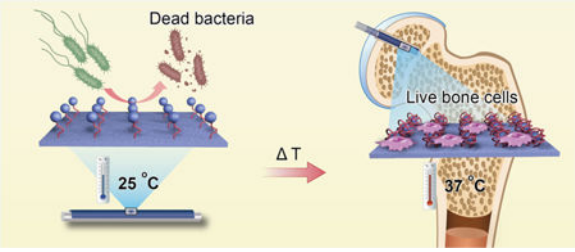

Keywords

antimicrobial peptides; temperature responsive; click chemistry; biocompatibility; implants

1. INTRODUCTION

Bacterial infection is a predominant medical complication on the implants.[1,2] To decrease it, the most efficient way is to construct a surface with antimicrobial agents, such as Ag, quaternary ammonium, and antibiotics, on the implants. However, these agents do not satisfy the clinical requirements because they can cause cytotoxicity[3] and drug resistance.[4] Antimicrobial peptides (AMPs) are more promising antimicrobial agents because they can resist the infection by more types of bacteria and even by fungi.[5] They can penetrate the bacterial cell membrane and thus could fight against drug-resistant bacteria.[6,7] Hence, surface modification with AMPs is an approach to the antimicrobial implants.

However, AMP is cytotoxicity[8-10] due to their nonspecific membrane selectivity. The AMP-modificated surfaces presented high antimicrobial activity but with low cytotoxicity toward mammalian cells[11-13], [-] while implants, such as vascular stents[14] and bone repair materials, [15-16] demand high in vivo biocompatibility. The low cytotoxicity of AMPs largely prohibited the application of AMPs. In order to improve the biocompatibility of AMPs, it is general to introduce some biologically active molecules which are suitable for cell growth, such as the RGD peptide. Here, we show an innovative approach to exploring the antibacterial property of AMPs but improving their biocompatibility with stimuli-responsive smart material without biologically active molecules. Stimuli-responsive smart material, a very promising material, has gained widespread concerns.[17,18] Their behaviors could respond to external stimuli, such as temperature, pH, light, and so on.[19-21] Because of the difference in temperature between the operational environment and living body, it is suited to control the

exposure of AMPs with external stimuli. Namely, we design the implant surface in such a way that AMPs are exposed to perform antibacterial function at room temperature, where the implants are usually stored and operated but hidden inside the surface to not to cause cytotoxicity at body temperature after implantation.

Briefly, we constructed such a smart surface by conjugating an AMP (HHC36, KRWWKWWRR) to the chain of a temperature-responsive polymer, poly(*N*-isopropylacrylamide) (pNI- PAM) through click chemistry (Scheme 1a). In addition, the antimicrobial activity and biocompatibility of the surface in vitro and in vivo were studied. HHC36 is chosen because it is a short peptide with a high antimicrobial activity.[22,23] The temperature-responsive polymer is chosen pNIPAM because its low critical solution temperature (LCST) is ~32 °C.[24,25] Below LCST (e.g., room temperature), pNIPAM is flexible, allowing its chain to be extended to expose AMPs and making the implants antibacterial. Above LCST (e.g., body temperature), pNIPAM is collapsed because of intramolecular H-bonding, allowing its chain to hide AMPs inside the surface, making it unavailable to the surroundings and thus minimizing the cytotoxicity (Scheme 1b).

2. RESULTS AND DISCUSSION

2.1. Preparation and Characterization of the AMP-Functionalized Surface.

To prepare an AMP functional surface, we first formed a polydopamine surface on the titanium (Ti) implants, on which pNIPAM with the uniform molecular weight (M_n) was formed through ATRP. Then, we conjugated an AMP (KRWWKWWRR) with the chain of pNIPAM click- chemically through Cu(I)-catalyzed azide-alkyne cycloaddition, forming Ti-pNIPAM-AMP (Scheme 1).

The IR spectra results (Figure 1) indicated that we had synthesized pNIPAM successfully. The peaks at 1540 cm^{-1} for the secondary amide —N—H stretching (amide II band), 1650 cm^{-1} for the primary amide —C=O— stretching (amide I band), 2971 cm^{-1} for the -CH_3- asymmetric stretching, 3298 cm^{-1} for the secondary amide -N-H stretching were observed on pNIPAM, which was consistent with previous literature about the synthesized pNIPAM.[26]

Then, the AMP-functionalized surface was characterized with X-ray photoelectron spectroscopy (XPS) (Figure S1). The N 1s high-resolution spectra of the surfaces after each step proved that AMP-functionalized surfaces were prepared successfully. In order to understand the surface compositions, the C/N ratio of Ti-AMP, Ti-pNIPAM, and Ti-pNIPAM-AMP were analyzed from the XPS spectra (Table S1). The C/N ratio ofTi-pNIPAM was 5.88, which was very close to the theoretical C/N ratio of pNIPAM, indicating that pNIPAM brush almost completely covered the surface. Ti-pNIPAM-AMP presented the lowest C/ N ratio, which was closer to the theoretical C/N ratio of AMP than that of Ti-AMP. This indicated that there were more AMP molecules on Ti-pNIPAM-AMP than Ti-AMP. The surface mass density of grafted AMP on Ti-pNIPAM-AMP was calculated to be about 641 ng/cm^2 from quartz crystal microbalance (QCM) analysis (Figure S2).

2.2. Temperature-Responsive Surface.

Under the temperature change cycles, the Ti-pNIPAM-AMP surface was found to be temperature-responsive. During the temperature change between 37 and 25 °C, the samples with pNIPAM showed a reversible change of contact angle, but the samples without pNIPAM did not (Figure 2a). QCM with dissipation (QCM-D) monitoring results also demonstrated a reversible change of the balanced frequency change (ΔF) (Figure 2b). When the temperature was changed from 37 to 25 °C at the first cycle, the change in ΔF for Ti and Ti-AMP is −68.6 and −71.1 Hz, which were very close. Also, the change in ΔF could be returned back to almost 0 Hz when the temperature was changed back from 25 to 37 °C. A similar curve appeared at the second and third cycles. These changes in ΔF could be attributed to the quartz's response to temperature due to the absence of temperature-sensitive pNIPAM on the two surfaces. After pNIPAM was introduced to the surface, the corresponding change in ΔF was −110.9 and −85.2 Hz for Ti-pNIPAM and Ti- pNIPAM-AMP, respectively. Such an increased change was responsive to a temperature change from 37 to 25 °C for pNIPAM-bearing surfaces compared to the nonbearing counter-parts because pNIPAM could absorb water through forming H- bonding with water, making its conformational extension to the surroundings. Ti-pNIPAM-AMP showed a smaller change in ΔF than Ti-pNIPAM between 37 and 25 °C, indicating that the amount of adsorbed water on Ti-pNIPAM-AMP was less than that on Ti-pNIPAM (Figure 2b), probably because the presence of AMP blocks pNIPAM from binding water molecules. When temperature was changed from 25 to 37 °C, the increased change in ΔF between the surfaces with and without pNIPAM disappeared, indicating that the hydration water was extruded as pNIPAM was collapsed at 37 °C. All these data further confirm the successful construction of Ti-pNIPAM-AMP.

2.3. Temperature-Controlled Exposure and Hiding of AMPs on the Surface.

To evaluate the exposure of the AMP response with temperature on the Ti-pNIPAM-AMP, AMP was replaced with a biotin-labeled molecule (biotin-PEG4-alkyne).

After incubation with fluorescein isothiocyanate (FITC)-labeled avidin at 25 °C, strong fluorescence was observed on the surface (Figure 3a) because of the exposure of biotin for recognizing

FITC-labeled avidin. However, the fluorescence nearly disappeared when the same surface was incubated at 37 °C (Figure 3b), indicating that the biotin-labeled molecule was not exposed to the environment and thus not available for recognizing FITC- labeled avidin. These data suggested that the AMP was exposed at a temperature below LCST, whereas they were buried inside pNIPAM and not exposed to the external environment at a temperature above LCST (Scheme 1b).

2.4. Antimicrobial Activity and Biocompatibilty in Vitro.

Free AMP showed a low concentration of minimum inhibitory concentration (MIC) against *Staphylococcus aureus (S. aureus)* and *Escherichia coli (E. coli)* (Figure S3). The MIC of the PraHHC36 against *S. aureus* and *E. coli* was found to be between 8-10 and 6-8 μM, respectively. Then, we analyzed the quantitative antimicrobial activity of the surfaces at

different *T's* with an agar plate method after incubation against *S. aureus* and *E. coli* for 2 h (Figure 4a). Interestingly, the antibacterial activity of Ti-pNIPAM-AMP against *S. aureus* was improved from 30.5 to 94.4% when temperature changed from 37 to 25 °C. Also, that against *E. coli* was improved from 32.5 to 95.1%. No residual antimicrobial Cu ions and bromide ions were observed on Ti- pNIPAM-AMP (Figure S4), which indicated that the antimicrobial activity of Ti-pNIPAM-AMP was contributed from AMPs. Meanwhile, antibacterial study using free AMP (Figure 4b) showed that AMP almost killed 100% of bacteria at both 25 and 37 °C. Therefore, the difference in the antibacterial activity of Ti-pNIPAM-AMP at both 25 and 37 °C further confirmed our hypothesis that this surface exposed AMP at $T <$ LCST, while buried AMP at $T >$ LCST. The flexible conformation of pNIPAM chains at 25 °C improved the accessibility of the AMP motif, making AMP easier to contact bacteria and kill them. Ti- pNIPAM and Ti-AMP could not kill bacteria at both 25 and 37 °C. Ti-pNIPAM could not kill bacteria because of the lack of antibacterial agents. Though Ti-AMP was incorporated with antibacterial agents, its AMP was not connected to the surface through a flexible linker, making it unable to perform antibacterial functions.[27]

We further analyzed the antimicrobial activity of the surfaces with the LIVE/DEAD method (Figures 5 and S5). There were many live bacteria (green fluorescence) but almost no dead bacteria on Ti and Ti-pNIPAM at both 37 and 25 °C. A number of dead bacteria (red fluorescence) with some live bacteria (green fluorescence) appeared on Ti-AMP and Ti-pNIPAM at 25 °C. However, much more dead bacteria (red fluorescence) were observed on Ti-pNIPAM-AMP than on Ti-AMP at 25 °C. The Ti-pNIPAM-AMP surface exhibited a reduced antibacterial behavior at 37 °C compared to that at room temperature. The results also indicated that the antimicrobial activity of Ti- pNIPAM-AMP could be tuned by changing temperature.

The biocompatibility of free AMPs (HHC36) was tested with BMSC (Figure S6), and the results showed that free AMPs displayed some cytotoxicity after incubation with BMSCs for 24 h at MIC. The results are similar with the previous study as they showed that AMPs were low cytotoxic.[6,28] Interestingly, Ti- pNIPAM-AMP not only showed a high antimicrobial activity at 25 °C, but also exhibited improved biocompatibility for the adhesion and proliferation of bone marrow derived stem cells (BMSCs) at 37 °C. Cell counting kit-8 (CCK-8) assay showed that after incubation with BMSCs for 2 d, the viability of the cells on Ti-pNIPAM-AMP was about 1.30,1.24, and 1.21 times those of Ti, Ti-pNIPAM, and Ti-AMP, respectively (Figure 6a). The results of the morphology of BMSCs were consistent with CCK- 8 assay results (Figure 6b). BMSCs at the highest density appeared on Ti-pNIPAM-AMP. Also, the BMSCs were spread well on Ti-pNIPAM-AMP as stretched cytoskeleton and round nucleus were observed. The results indicated that dual functional Ti-pNIPAM-AMP presented the best biocompatibility among the four surfaces, which was caused by the hiding of AMP. The collapsed conformation of pNIPAM chains buried most AMPs at 37 °C in the surface of Ti-pNIPAM-AMP, limiting the accessibility of the low cytotoxic AMP motifs. Also, the hydrophobic environment formed by the collapse of pNIPAM was suggested to contribute to the improved biocompatibility of Ti-pNIPAM-AMP at 37 °C as it is suitable for cell growth according to a previous study.[29] The hydrophobic environment cause by the collapse of pNIPAM also made Ti-pNIPAM present a better biocompatibility than Ti. However, Ti-AMP presented a better biocompatibility than Ti. This

discrepancy may be attributed to the absence of a flexible linker on Ti-AMP, which made AMPs hard to access cells.

When the implant was in contact with blood after implantation, the red blood cells may be damaged and may release red blood globulin, causing hemolysis. The hemolysis activity of the surfaces was tested with rabbit red blood cells. The surfaces showed a lower hemolysis activity, and the hemolysis activity of Ti, Ti-pNIPAM, Ti-AMP, and Ti-pNIPAM-AMP was 2.01 ± 0.44, 1.27 ± 1.7, 2.23 ± 2.25, and 3.35 ± 1.77%, respectively (Figure 7). Though the hemolysis activity of Ti- pNIPAM-AMP was increased slightly, the value was still below the acceptable value of 5% and met the medical adsorbent standard of China (ISO 10994.4: 2002). These results showed that Ti-pNIPAM-AMP presented good blood compatibility.

2.5. Antimicrobial Activity and Biocompatibility in Vivo.

The antimicrobial activity of a rod-like Ti-pNIPAM-AMP implant in vivo was evaluated by an infection rabbit model (Figure 8). Before implantation into tibias, the implants were incubated in the clinically relevant *S. aureus* bacteria solution (10^7 cfu/mL) for 2 h at room temperature (RT). After implantation for 7 d, the samples were explanted from the tibias and rolled over a blood agar plate for semi-quantification of bacteria adhered on the plate (Figure 8a). The blood agar images showed that many bacteria (the yellow spots) appeared on Ti, but only a few were observed on Ti-pNIPAM-AMP, indicating that Ti-pNIPAM-AMP presented a high antimicrobial activity before being implanted. The quantitative antimicrobial activity of the surfaces of explanted samples (Figure 8b) and their surrounding tissues (Figure 8c) showed the excellent antimicrobial activity of Ti-pNIPAM-AMP in vivo, consistent with the blood agar results (Figure 8a). Nearly 100% of the bacteria on the surface of Ti-pNIPAM-AMP were killed. These results showed that even challenged with bacteria solution before implantation, Ti-pNIPAM-AMP could kill the bacteria at RT, making few bacteria brought to rabbit model after implantation and decreasing bacterial infection in vivo.

We further study the morphology of tissues and bacterial residues with hematoxylin and eosin (H&E; Figure 8d) and Giemsa (Figure 8e) staining. H&E staining showed that Ti presented the destruction ofcortical and cancellous bone as well as tissues infiltration with a large number of inflammatory cells (yellow arrows) such as lymphocytes, monocytes, and neutrophils. Also, multinucleated osteoclasts (blue arrows) were detected on Ti, suggesting the presence of bacterial infection and bone resorption.[30] Meanwhile, Giemsa staining results indicated that the bacterial infection occurred on Ti because there were a lot of bacteria (red arrows) around Ti implants.[31] However, Ti-pNIPAM-AMP presented little destruction of cortical and cancellous bone and much fewer inflammatory cells. Moreover, a number of live bone cells (black arrows), but not signs of bacterial infection, were observed on Ti-pNIPAM-AMP. These results indicated that the temperature-sensitive surface we prepared presented not only an excellent antimicrobial activity at RT before implantation, but also an increased biocompatibility in vivo after implantation even when it was challenged with bacteria before implantation. The exposure of AMP on Ti-pNIPAM-AMP enabled the implants to kill the bacteria at RT before implantation, making no bacterial infection after implantation. When Ti-pNIPAM- AMP was implanted in vivo, the body

temperature made the AMP buried inside the surface on Ti-pNIPAM-AMP, decreasing the toxicity of the AMP to normal cells and increasing the biocompatibility in vivo.

3. CONCLUSIONS

We have developed a smart surface which can control the exposure AMPs through the temperature-controlled conformational change of pNIPAM chains, resulting in the development of an implant that shows an excellent antimicrobial activity at RT and an increased biocompatibility at body temperature. During the storage and usage of the implants at room temperature, the bacterial adhesion on the surface will contribute to bacterial infection. Our designed surface could exhibit an antimicrobial activity at this stage to inhibit the adhesion of the bacteria and kill them. After implantation into the body, the surface presents an improved biocompatibility. This work moves a step forward into the construction ofsmart functional surfaces that can switch properties through the temperature-controlled exposure or hiding of various drug molecules.

4. MATERIALS AND METHODS

4.1. Materials.

Titanium rods were purchased from Tsinghua- Foxconn Nanotechnology Research Center. Dopamine, NIPAM, CuBr, sodium ascorbate, and tris(3-hydroxypro-pyltriazolylmethyl)amine (THPTA, 95%, ligand) were purchased from Sigma-Aldrich. HHC36, PraHHC36, and biotin-PEG4-alkyne were purchased from GL Biochemical (shanghai) Co., Ltd. Tri-HCl was purchased from Shanghai Bioscience Co., Ltd. 2-Bromoisobutyryl bromide was purchased from Aladdin. Triethylamine (TEA) was acquired from Guangzhou chemical reagents factory. Tris[2-dimethylamino]ethyl]- amine was purchased from Tokyo Chemical Industry Co., Ltd. NaN_3 was purchased from Tianjin Fuchen chemical reagents factory. Ethylenediaminetetraacetic acid (EDTA) and $CuSO_4{\cdot}5H_2O$ were acquired from Guangdong Guanghua Technology Co., Ltd. All the reagents related to cell test and assay were purchased from Sigma.

4.2. Preparation of pNIPAM Brushes on Ti.

The titanium rods were cleaned with an ultrasonic bath in ethanol and the water for 15 min, respectively. After being dried with nitrogen flow, the substrates (Ti) were immersed in 2 mg/mL of dopamine solution with Tri-HCl (10 mM, pH 8.5) for 30 min. After being treated with an ultrasonic bath in ethanol for 15 min, the substrates (abbreviation as Ti-PDA) were dried with nitrogen flow and immersed in 1 mL TEA and 10 mL dichloromethane, followed by adding 800 μL 2-bromoisobutyryl bromide dropwise into the solution at the ice bath for 2 h and at the room temperature for 12 h in order to generate Ti-Br. Then, the substrates were treated with an ultrasonic bath in ethanol for 15 min and dried with nitrogen flow. The polymerization of NIPAM was performed in a degassed NIPAM solution (1.13 g, 10 mmol) with CuBr (14.35 mg, 0.1 mmol) and tris[2-dimethylamino]ethyl]amine (50 μL, 0.2 mmol) in methanol/water mixed solvent (5:5, v/v) for 2 h. The substrates were treated with an ultrasonic bath in water for 15 min followed by a nitrogen flow and abbreviated as Ti-

pNIPAM. The reacted solution was collected, dialyzed for 5 days, and then freeze-dried to obtain pNIPAM.

4.3. Functional AMP Grafting on pNIPAM Brushes of Ti- pNIPAM.

Before click chemistry conjugation, Ti-Br and Ti-pNIPAM were azidated with NaN_3 to introduce the reaction site of click chemistry. Briefly, Ti-Br and Ti-pNIPAM were reacted with 0.25 g NaN_3 in dimethylformamide and water-mixed solvent (8:2, v/v) at 60 °C for 12 h and treated with an ultrasonic bath in water for 15 min, followed by a N_2 flow to form new substrates, termed Ti-N_3 and Ti- PNIPAM-N_3, respectively. Then, the AMP was grafted on the surface via click chemistry in the solution of AMP (0.1 mM), THPTA (0.2 mM), $CuSO_4$ (0.1 mM), and sodium ascorbates (5 mM) in a mixture of ethanol and water (3:7, v/v). After 3 h, the substrates were immersed in an EDTA solution (5 mM). Then, they were treated with an ultrasonic bath in water for 15 min, followed by a N_2 flow and abbreviated as Ti-AMP and Ti-pNIPAM-AMP, respectively.

4.4. Infrared Spectroscopy.

The pNIPAM was pressed into discs with potassium bromide and detected with a Fourier transform infrared (FT-IR) spectroscopy analyzer (VECTOR-22, Bruker, Germany). The spectroscopy spectra (500-4000 cm^{-1}) were collected at 4.0 cm^{-1} resolution with 32 scans.

4.5. XPS Assay.

The surfaces were measured by a photoelectron spectrometer (AXIS ULTR DLD, Kratos, England) with an Al Kα (1486.4eV) monochromaticX-raysourceatapressureof 2×10^{-9} Torr and a scan area of 0.7×0.3 mm^2. Analyses consisted of a survey scan performed at a pass energy of 160 eV to identify all the species present, followed by high resolutions scans (40 eV) of the species of interest.

4.6. Static Contact Angle Measurement.

The static contact angle of the surfaces was characterized with a contact angle goniometer (OCA15, DADAPHYSICS, England) at 25 and at 37 °C, and 1.00 μL of distilled water was dropped onto the surface through a stainless steel needle at a rate of 1.0 μL/s. The results are mean values calculated from five independent measurements on different points of the surfaces.

4.7. Conformational Change ofpNIPAM Chains in Response to Temperature.

The conformation of pNIPAM chains as a function of temperature was characterized with QCM-D monitoring (Q-Sense E4, Biolin, Sweden). Briefly, the surfaces maintained a baseline in phosphate buffer saline (PBS) at 37 °C. Then, the temperature was changed to 25 °C for 20 min. When the frequency was balanced, the temperature was adjusted to 37 °C until the frequency was balanced again. The process was repeated for three cycles.

4.8. Fluorescence Microscopy.

The surfaces were immersed in avidin-labeled FITC solution with a concentration of 0.1 mg/mL for 15 min in the dark at 25 and 37 °C and then rinsed with water at 25 and 37 °C,

respectively. The fluorescence of the surfaces was detected by fluorescence microscopy (Eclipse Ti-U, Nikon).

4.9. Antimicrobial Assayand Bacterial Culture.

Asingle colony of *S. aureus* (ATCC 29213) or *E. coli* (ATCC 35150) was inoculated in Luria-Bertani (LB) medium overnight at 37 °C. After adding 100 μL *S. aureus* (ATCC 29213) or *E. coli* (ATCC 35150) suspension to 5 mL of fresh LB medium, *S. aureus* (ATCC 29213) or *E. coli* (ATCC 35150) was incubated for 5 h with shaking (250 rpm) at 37 °C to achieve mid- log-phase growth.

4.9.1. Colony Counting Assay of the Antimicrobial Activity.—The antimicrobial activity of AMP solution (10, 50, and 100 μM) at 25 and 37 °C was tested with the *S. aureus* (or *E. coli)* suspension (1×10^7 cfu/ mL in PBS). After incubation for 2 h, the antimicrobial activity was evaluated with agar plates by a serial dilution method. The surfaces (0.5 cm × 0.5 cm) were sterilized by 70% isopropyl alcohol for 2 h, placed in a 48-well culture plate, and rinsed with PBS buffer for 3 times. Then, 10 μL of the bacterial suspension (1×10^7 cfu/mL in PBS) was added into each surface and incubated at 25 and 37 °C for 2 h, respectively. After 990 μL PBS buffer was added, the surfaces and the PBS buffer were put in a sterile centrifuge tube and treated with an ultrasonic bath for 10 min to detach the bacteria. Then, the qualitative antibacterial behaviors of the surfaces were evaluated by a serial dilution method with agar plates. The method to test the MIC of AMPs against *S. aureus* and *E. coli* is shown in the Supporting Information.

4.9.2. LIVE/DEAD Staining Assay.—The viability of bacteria adhering onto the surfaces was tested with the LIVE/DEAD staining.[32-34] The reagent mixture was obtained by mixing the equal amount of fluorescein diacetate solution (0.5%) and propidium iodide solution (0.5%) and was added to the surfaces. After incubation for 15 min at the room temperature in the dark environment, the surfaces were rinsed with distilled water, and observed by confocal laser scanning microscope (TCS SP8, Leica, Germany) on the randomly chosen locations. Bacteria with intact cell membranes would be stained with green fluorescence, whereas those with damaged membranes would be stained with red fluorescence.

4.10. Biocompatibility of the Samples.

Rat bone marrow mesenchymal stem cells (BMSC, CRL-12424, ATCC, USA) were used to study the biocompatibility of the samples. The cells were cultured in a Dulbecco's modified Eagle medium (DMEM, Gibco, USA) containing 10% fetal bovine serum (FBS, Gibco, USA) and at 37 °C with a 5% CO_2 atmosphere. The medium was replaced every 2 days. All surfaces (0.5 cm X 0.5 cm) were sterilized with 70% isopropyl alcohol for 2 h and placed individually into new 48-well plates. Then, the surfaces were seeded with BMSCs (20 000/ mL).

4.10.1. Cellular Viability.—After incubation for 2 days, the cellular viability of the surfaces was tested with CCK-8 assay. The medium was removed. Then, 200 μL DMEM with 10% FBS and 20 μL Cell Counting Kit-8 (CCK-8) reagent were mixed and added to

the surfaces. After incubation for 1 h, the optical density (OD) values at450 nmwere measured with an ELISA plate reader (Varioskan Flash 3001, Thermo, Finland).

4.10.2. Morphology of Cells.—After incubation for 2 days, the morphology of cells was observed by a confocal laser scanning microscope. The surfaces were rinsed with PBS at the same temperature and then fixed with 4% glutaraldehyde at —4 °C overnight. After being rinsed with PBS 3 times, the surfaces were immersed in FITC solution with a concentration of 0.1 mg/mL in the dark for 30 min, followed by rinsing with PBS. The surfaces were stained with 4',6-diamidino-2- phenylindole for 5 min in the dark, rinsed with PBS, and observed by a confocal laser scanning microscope (Leica TCS SP8, Germany). The method to test the biocompatibility of free AMPs is shown in the Supporting Information.

4.11. Hemolytic Activity of the Surfaces.

The hemolytic activity of the surfaces was tested with rabbit red blood cells. At first, the rabbit red blood cells were purified by the followingprocedure: 5 mL of rabbit blood was added to 10 mL of PBS. After mixing, the suspension was centrifuged at 800*g* for 10 min. Then, the supernatant was discarded, and 1 mL of PBS was added again. After the process was repeated 5 times, Ti-AMP, Ti-pNIPAM, and Ti-pNIPAM-AMP were placed in a 48-well plate and incubated with 500 μL 5% red blood cell solution (dissolved in PBS) for 3 h. The red blood cells incubated with 0.1% Triton X-100 and PBS were used as a positive and negative control, respectively. Then, the red blood cell solution was collected and centrifuged at 800*g* for 10 min, followed by OD measurements at 540 nm with 100 μL of the supernatant in a 96-well plate.

The hemolysis value (*H*) of the surfaces was calculated from the equation below.

$$\mathrm{H} = 100\% \times \frac{A_{\mathrm{s}} - A_{\mathrm{n}}}{A_{\mathrm{p}} - A_{\mathrm{n}}}$$

where A_s, A_n, and A_p are the absorbance of the surfaces, negative control (PBS), and positive control (0.1% Triton X-100), respectively.

4.12. Antimicrobial Activity in Vivo and Infectious Rabbit Model.

Six 2.0 kg New Zealand albino rabbits were divided into two groups at random. The operation was performed on the left hind leg of the rabbits. Briefly, after the rabbits were anaesthetized with 3% pelltobarbitalum natricum solutions (in normal saline) and xylazine hydrochloride injection, their left hind leg was shaved, cleaned with 75% ethanol solution, and draped with sterile sheets. Then, the patellar ligament ofthe left tibia was divided, and the metaphysis part ofthe tibia was exposed. A 3.0 mm defect of medullary cavity was made with dental drill, followed by adding 100 μL of sodium morrhuate solution with 5% mass concentration. After the samples (Ti and Ti-pNIPAM-AMP) were immersed in the *S. aureus* (SA) solution (1×10^7 cfu/mL) for 2 h at the room temperature, they were implanted into the defect of medullary cavity and the defect site was sealed with a bone candle. Then, the

patellar ligament and the skin were closed with the suture line. After surgery for 7 days, the rabbits were euthanized and the tibias were obtained under an aseptic environment.

4.12.1. Microbiological Evaluation.—The samples (Ti and Ti- pNIPAM-AMP) were explanted from the tibias and rolled over blood agar for semi-quantification ofbacterial adhesion on the surfaces. Then, they were placed in 5 mL nutrient broth and treated with an ultrasonic bath for 10 min to detach the bacteria. The qualitative antibacterial activity of the samples on the surface was evaluated by a serial dilution method with agar plates. After the substrates were explanted, tibias were divided into two equal parts. One part was freeze-dried and grinded to powder bones (and another part was used in the experiments in the next sub-section), and 1 g of powdered bones was agitated in 10 mL of normal saline for 3 min. After centrifugation at 1000 rpm for 10 s, 0.1 mL of the supernatant was obtained and used to evaluate the antimicrobial activity of the samples around the tissue by a serial dilution method with agar plates.

4.12.2. Histopathological Evaluation.—The remaining tibia of each samples was fixed in 4% paraformaldehyde. After 24 h, the samples were washed with water for 24 h. Then, the samples were decalcified in 10% EDTA solution for 4 weeks and paraffin-embedded. Longitudinal sections in a sagittal plane were cut into 5 μm by a microtome and dried on the slides. H&E and Giemsa staining were employed to evaluate the morphology of tissues and the bacterial residues.

Supplementary Material

Refer to Web version on PubMed Central for supplementary material.

ACKNOWLEDGMENTS

This work was supported by the National Key R&D Program of China (2018YFC1105402 and 2016YFA0100900), the National Natural Science Foundation of China (51232002, 31771027 and 51673168), Guangzhou Important Scientific and Technological Special Project (201508020123), Science and Technology Program ofGuangzhou (201804020060), and Pearl River Nova Program of Guangzhou (201806010156). Y.Z. and C.B.M. would like to acknowledge the financial support of National Institutes of Health (CA195607).

REFERENCES

(1). Zhan J; Wang L; Liu S; Chen J; Ren L; Wang Y Antimicrobial Hyaluronic Acid/ Poly(amidoamine) Dendrimer Multi layer on Poly(3-hydroxybutyrate-co-4-hydroxybutyrate) Prepared by a Layer-by-Layer Self-Assembly Method. ACS Appl. Mater. Interfaces 2015, 7, 13876–13881. [PubMed: 26061897]

(2). Darouiche RO Current concepts - Treatment of infections associated with surgical implants. N. Engl. J. Med. 2004, 350, 1422–1429. [PubMed: 15070792]

(3). Kennedy AJ; Hull MS; Bednar AJ; Goss JD; Gunter JC; Bouldin JL; Vikesland PJ; Steevens JA Fractionating Nanosilver: Importance for Determining Toxicity to Aquatic Test Organisms. Environ. Sci. Technol 2010, 44, 9571–9577. [PubMed: 21082828]

(4). Levy SB; Marshall B Antibacterial resistance worldwide: causes, challenges and responses. Nat. Med. 2004, 10, S122. [PubMed: 15577930]

(5). Wang L; Chen J; Shi L; Shi Z; Ren L; Wang Y The promotion of antimicrobial activity on silicon substrates using a “click” immobilized short peptide. Chem. Commun. 2014, 50, 975–977.

(6). Chen W-Y; Chang H-Y; Lu J-K; Huang Y-C; Harroun SG; Tseng Y-T; Li Y-J; Huang C-C; Chang H-T Self-Assembly of Antimicrobial Peptides on Gold Nanodots: Against Multidrug- Resistant Bacteria and Wound-Healing Application. Adv. Funct. Mater. 2015, 25, 7189–7199.

(7). Roy I; Shetty D; Hota R; Baek K; Kim J; Kim C; Kappert S; Kim K A Multifunctional Subphthalocyanine Nanosphere for Targeting, Labeling, and Killing of Antibiotic-Resistant Bacteria. Angew. Chem. 2015, 127, 15367–15370.

(8). Xiong M; Han Z; Song Z; Yu J; Ying H; Yin L; Cheng J Bacteria-Assisted Activation of Antimicrobial Polypeptides by a Random-Coil to Helix Transition. Angew. Chem., Int. Ed. 2017, 56, 10826–10829.

(9). Zhu X; Dong N; Wang Z; Ma Z; Zhang L; Ma Q; Shan A Design of imperfectly amphipathic a-helical antimicrobial peptides with enhanced cell selectivity. Acta Biomater. 2014, 10, 244–257. [PubMed: 24021230]

(10). Sahariah P; Sorensen KK; Hjálmarsdóttir MÁ; Sigurjónsson ÓE; Jensen KJ; Masson M; Thygesen MB Antimicrobial peptide shows enhanced activity and reduced toxicity upon grafting to chitosan polymers. Chem. Commun. 2015, 51, 11611–11614.

(11). Wang L; Chen J; Shi L; Shi Z; Ren L; Wang Y The promotion of antimicrobial activity on silicon substrates using a “click” immobilized short peptide. Chem. Commun. 2014, 50, 975–977.

(12). Rai A; Pinto S; Evangelista MB; Gil H; Kallip S; Ferreira MGS; Ferreira L High-density antimicrobial peptide coating with broad activity and low cytotoxicity against human cells. Acta Biomater. 2016, 33, 64–77. [PubMed: 26821340]

(13). Lin W; Junjian C; Chengzhi C; Lin S; Sa L; Li R; Yingjun W Multi-biofunctionalization of a titanium surface with a mixture of peptides to achieve excellent antimicrobial activity and biocompatibility. J. Mater. Chem. B 2015, 3, 30–33.

(14). Waterhouse A; Yin Y; Wise SG; Bax DV; McKenzie DR; Bilek MMM; Weiss AS; Ng MKC The immobilization of recombinant human tropoelastin on metals using a plasma-activated coating to improve the bio compatibility of coronary stents. Biomaterials 2010, 31, 8332–8340. [PubMed: 20708259]

(15). Amin Yavari S; van der Stok J; Chai YC; Wauthle R; Tahmasebi Birgani Z; Habibovic P; Mulier M; Schrooten J; Weinans H; Zadpoor AA Bone regeneration performance ofsurface- treated porous titanium. Biomaterials 2014, 35, 6172–6181. [PubMed: 24811260]

(16). Lee Y-H; Bhattarai G; Park I-S; Kim G-R; Kim G-E; Lee M-H; Yi H-K Bone regeneration around N-acetyl cysteine-loaded nanotube titanium dental implant in rat mandible. Biomaterials 2013, 34, 10199–10208. [PubMed: 24054849]

(17). Cobo I; Li M; Sumerlin BS; Perrier S Smart hybrid materials by conjugation of responsive polymers to biomacromolecules. Nat. Mater. 2015, 14, 143–159. [PubMed: 25401924]

(18). Cobo I; Li M; Sumerlin BS; Perrier S Smart hybrid materials by conjugation of responsive polymers to biomacromolecules. Nat. Mater. 2014, 14, 143–159. [PubMed: 25401924]

(19). Huang X; Sun Y; Soh S Stimuli-Responsive Surfaces for Tunable and Reversible Control of Wettability. Adv. Mater. 2015, 27, 4062–4068. [PubMed: 26043083]

(20). Huang X; Sun Y; Soh S Stimuli-Responsive Surfaces for Tunable and Reversible Control of Wettability. Adv. Mater. 2015, 27, 4062–4068. [PubMed: 26043083]

(21). Sasikala ARK; GhavamiNejad A; Unnithan AR; Thomas RG; Moon M; Jeong YY; Park CH; Kim CS A smart magnetic nanoplatform for synergistic anticancer therapy: manoeuvring mussel-inspired functional magnetic nanoparticles for pH responsive anticancer drug delivery and hyperthermia. Nanoscale 2015, 7, 18119–18128. [PubMed: 26471016]

(22). He J; Chen J; Hu G; Wang L; Zheng J; Zhan J; Zhu Y; Zhong C; Shi X; Liu S; Wang Y; Ren L Immobilization of an antimicrobial peptide on silicon surface with stable activity by click chemistry. J. Mater. Chem. B 2018, 6, 68–74.

(23). Kazemzadeh-Narbat M; Lai BFL; Ding C; Kizhakkedathu JN; Hancock REW; Wang R Multilayered coating on titanium for controlled release of antimicrobial peptides for the prevention of implant-associated infections. Biomaterials 2013, 34, 5969–5977. [PubMed: 23680363]

(24). Belal K; Stoffelbach F; Lyskawa J; Fumagalli M; Hourdet D; Marcellan A; De Smet L; de la Rosa VR; Cooke G; Hoogenboom R; Woisel P Recognition-Mediated Hydrogel Swelling

Controlled by Interaction with a Negative Thermoresponsive LCST Polymer. Angew. Chem., Int. Ed. 2016, 55, 13974–13978.

(25). Jiang S; Liu F; Lerch A; Ionov L; Agarwal S Unusual and Superfast Temperature-Triggered Actuators. Adv. Mater. 2015, 27, 4865–4870. [PubMed: 26186175]

(26). Estillore NC; Park JY; Advincula RC Langmuir-Schaefer (LS) Macroinitiator Film Control on the Grafting of a Thermosensitive Polymer Brush via Surface Initiated-ATRP. Macromolecules 2010, 43, 6588–6598.

(27). Onaizi SA; Leong SSJ Tethering antimicrobial peptides: Current status and potential challenges. Biotechnol Adv. 2011, 29, 67–74. [PubMed: 20817088]

(28). Fjell CD; Hiss JA; Hancock REW; Schneider G Designing antimicrobial peptides: form follows function. Nat. Rev. Drug Discovery 2012, 11, 37–51.

(29). Schmidt S; Zeiser M; Hellweg T; Duschl C; Fery A; Möhwald H Adhesion and Mechanical Properties of PNIPAM Microgel Films and Their Potential Use as Switchable Cell Culture Substrates. Adv. Funct. Mater. 2010, 20, 3235–3243.

(30). Jin G; Qin H; Cao H; Qiao Y; Zhao Y; Peng X; Zhang X; Liu X; Chu PK Zn/Ag micro-galvanic couples formed on titanium and osseointegration effects in the presence of S. aureus. Biomaterials 2015, 65, 22–31. [PubMed: 26141835]

(31). Qin H; Cao H; Zhao Y; Zhu C; Cheng T; Wang Q; Peng X; Cheng M; Wang J; Jin G; Jiang Y; Zhang X; Liu X; Chu PK In vitro and in vivo anti-biofilm effects of silver nanoparticles immobilized on titanium. Biomaterials 2014, 35, 9114–9125. [PubMed: 25112937]

(32). Setyawati MI; Kutty RV; Tay CY; Yuan X; Xie J; Leong DT Novel Theranostic DNA Nanoscaffolds for the Simultaneous Detection and Killing of Escherichia coli and Staphylococcus aureus. ACSAppl Mater. Interfaces 2014, 6, 21822–21831.

(33). Zhan J; Wang L; Liu S; Chen J; Ren L; Wang Y Antimicrobial Hyaluronic Acid/ Poly(amidoamine) Dendrimer Multilayer on Poly(3-hydroxybutyrate-co-4-hydroxybutyrate) Prepared by a Layer-by-Layer Self-Assembly Method. ACS Appl Mater. Interfaces 2015, 7, 13876–13881. [PubMed: 26061897]

(34). Zheng K; Setyawati MI; Lim T-P; Leong DT; Xie J Antimicrobial Cluster Bombs: Silver Nanoclusters Packed with Daptomycin. ACS Nano 2016, 10, 7934–7942. [PubMed: 27494437]

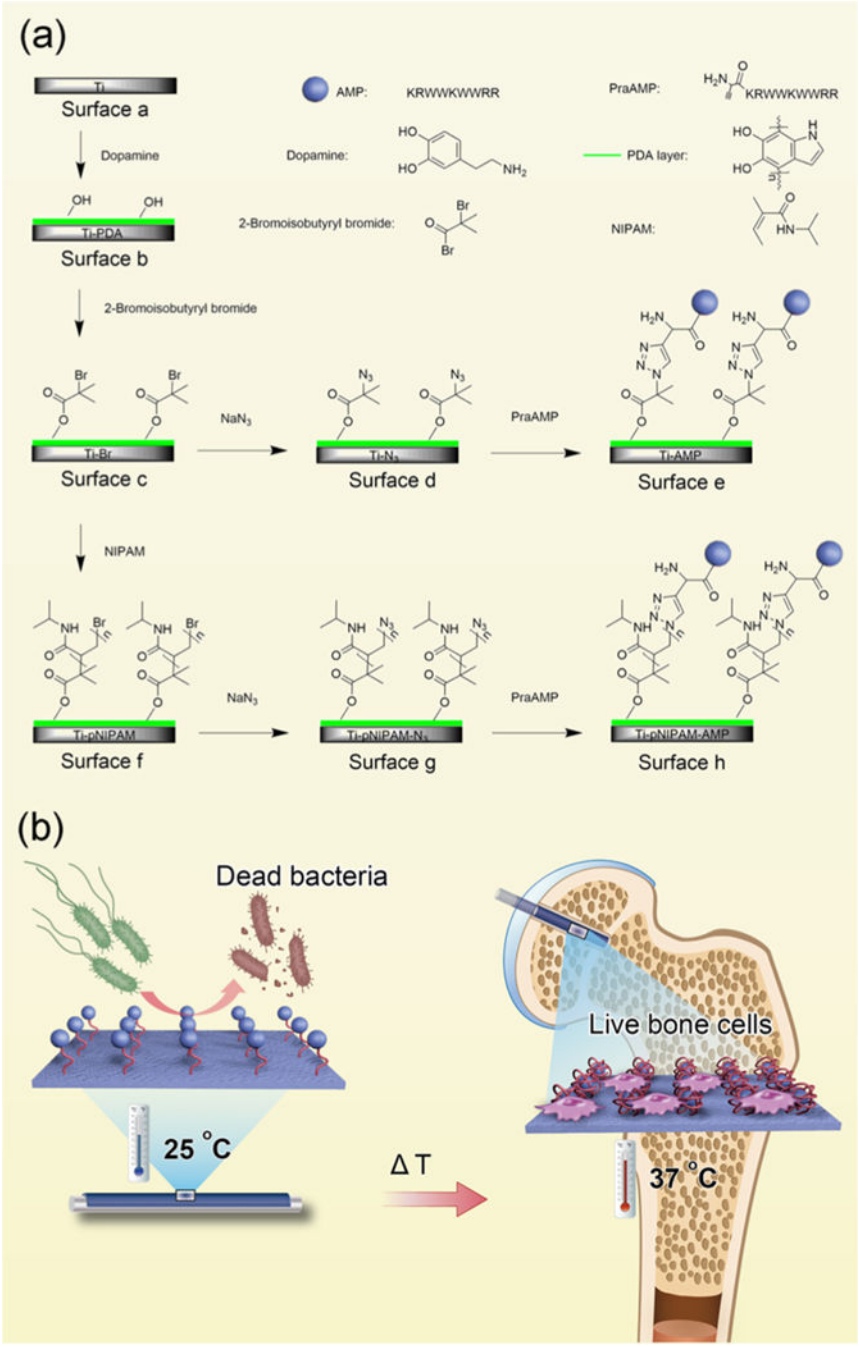

Scheme 1.

Scheme of Preparation and Effect of the Temperature-Sensitive Surfaces on Ti Substrates. (a) Surface Construction; Surface a (Ti) Was Treated with Dopamine To Form Surface b (Ti-PDA) Coated with Polydopamine (PDA); Then, Surface b Was Treated with 2-Bromoisobutyryl Bromide To Form Surface c (Ti-Br); By Click Chemistry, Surface c Was First Converted into Surface d (Ti-N_3) by Adding NaN_3, and Then into Surface e (Ti- AMP) by Adding praAMP (the AMP, KRWWKWWRR, Modified with L-Propargylglycine); Surface e (Ti-AMP) Contained AMP But Lacked pNIPAM; By Atom Transfer Radical

Polymerization (ATRP), pNIPAM with an LCST of 32 °C, Was Formed on Surface c To Generate Surface f (Ti- pNIPAM); By Click Chemistry, Surface f Was Converted First into Surface g (Ti-pNIPAM-N_3) by Adding NaN_3 and Then into Surface h (Ti-pNIPAM-AMP) by Adding praAMP. Surface f Contained AMP Conjugated to the Chain of pNIPAM; (b) Temperature-Sensitive Smart Behavior of Ti- pNIPAM-AMP; At T < LCST (e.g., Room Temperature), the Chain of pNIPAM is Extended, Enabling the AMP to be Exposed and Act as an Antibacterial Agent; At T > LCST (e.g., 37 °C), the Chain of pNIPAM is Condensed To Bury the AMP, Making AMP Unavailable for Causing the Cytotoxicity and Thus Improving the Biocompatibility of the Surface

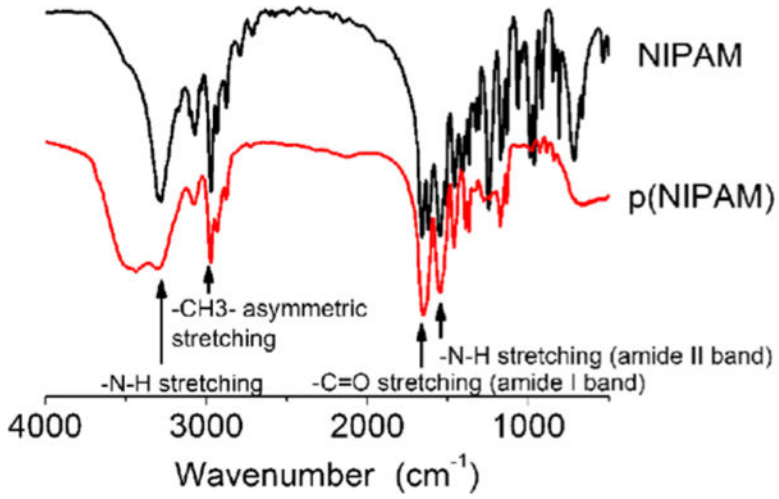

Figure 1.
IR spectra of NIPAM and pNIPAM.

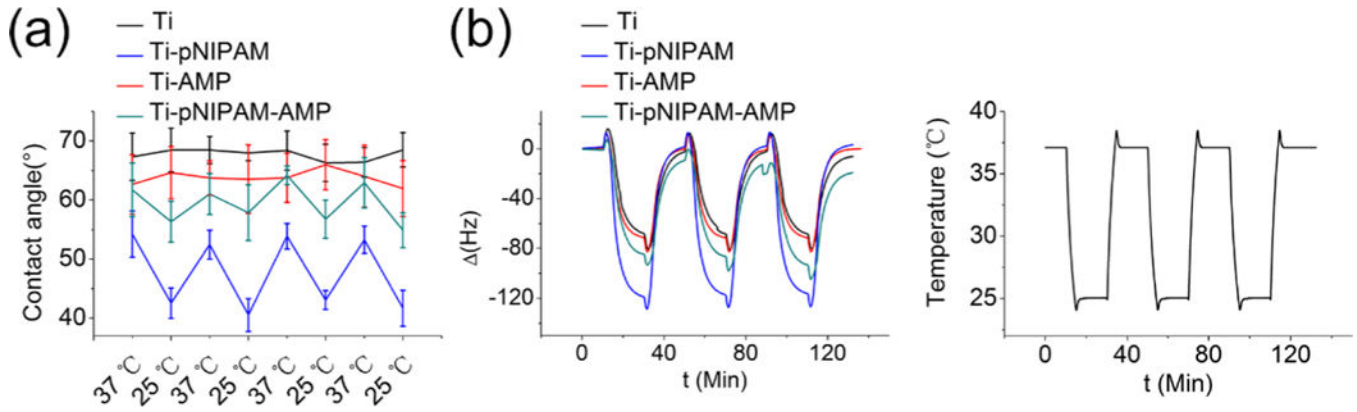

Figure 2.

Characterization of different surfaces by contact angle measurement and QCM-D analysis under a temperature change cycle, showing that the Ti-pNIPAM-AMP surface is temperature responsive. (a) Contact angle of the different surfaces at 25 and 37°C for 4 cycles. (b) QCM-D signal, the frequency change (Δ*F*), of different surfaces (left) and under a corresponding temperature cycle (right). The definition of different surfaces can be found in Scheme 1.

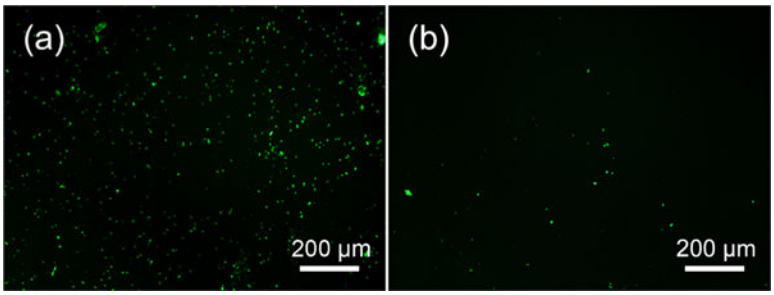

Figure 3.

Exposure and hiding of AMPs at lower and higher temperature, respectively. Fluorescence images of (biotin-alkynyl)- grafted Ti-pNIPAM-AMP incubated in avidin-conjugated FITC solution at 25 (a) and 37 °C (b). Green fluorescence indicated that the AMPs were exposed on the surface. These results showed that AMPs were exposed below LCST and hidden above LCST.

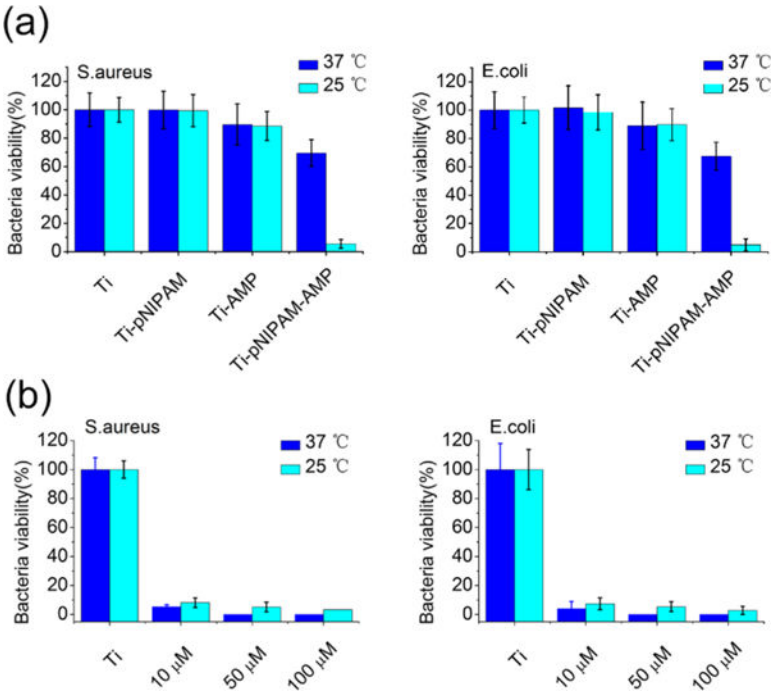

Figure 4.

Exposure of AMP's improved antibacterial behavior on Ti-pNIPAM-AMP. (a) Quantitative antibacterial activity of different surfaces after incubation agtainst *S.aureus* and *E.coli* for 2h with an agar plate method, suggesting the antimicrobial activity of the Ti-pNIPAM-AMP surface was responsive to tyemperature. Ti-pNIPAM-AMP presented the most antimicrobial activity among difference surfaces, in particular, when temperature was set at 25°C. (b) Antibacterial activity of free AMPs at different temperatures after incubation against *S.aureus* and *E.coli* for 2h. The results indicated that free AMP presented excellent antimicrobial activity at different temperatures.

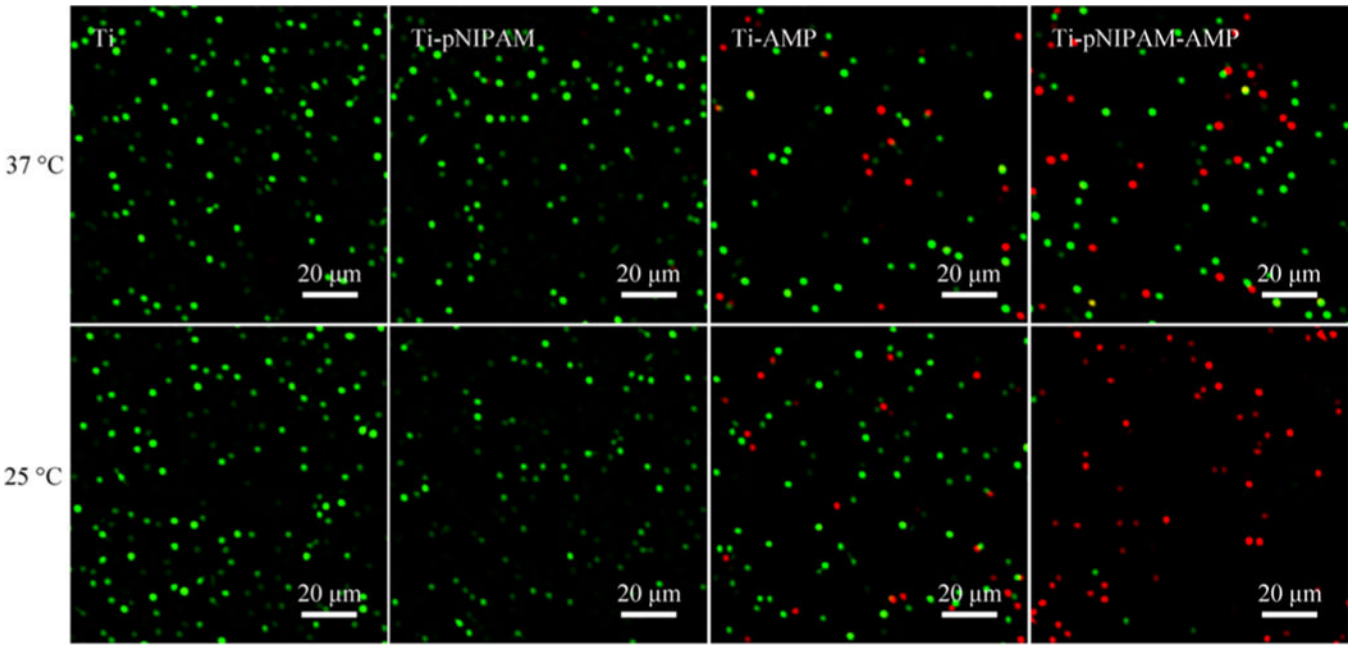

Figure 5.

Dead/live image of different surfaces after incubation against *S.aureus* for 2h at 37 and 25°C. The green fluorescence means live bacteria and the red fluorescence means dead bacteria. The results showed that the Ti-pNIPAM-AMP surface could kill bacteria at room temperature.

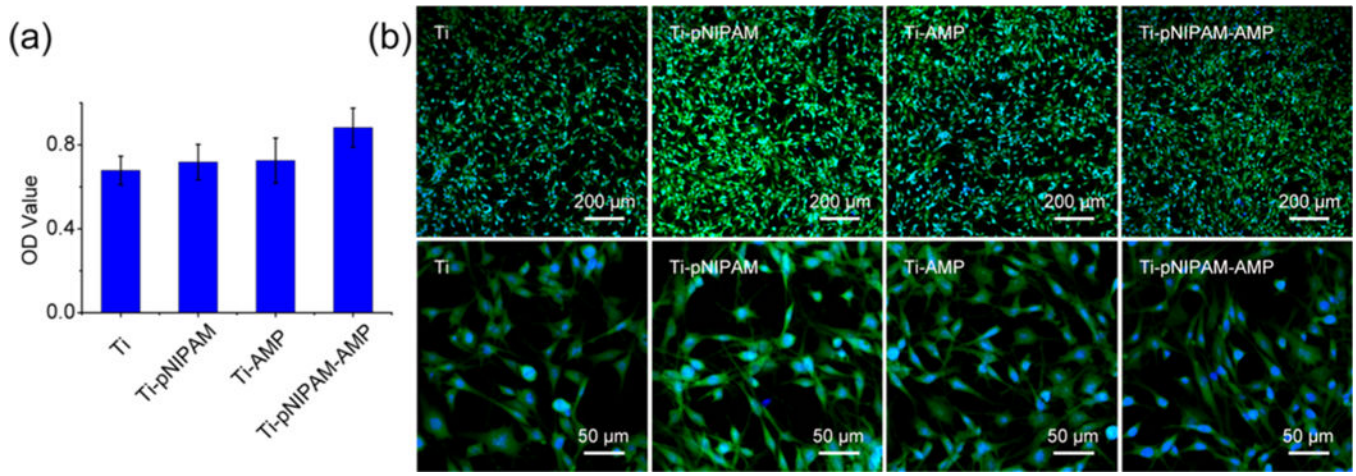

Figure 6.

Cellular viability and morphology of BMSCs on difference surface incubation for 2 d, showing the improved biocompatibility Ti-pNIPAM-AMP at 37° C. (a) CCK-8 assay of the viability of BMSCs on the different surfaces to evaluate their biocompatibility. (b) Morphology of BMSCs on the different surfaces was observed by confocal laser scanning microscope.

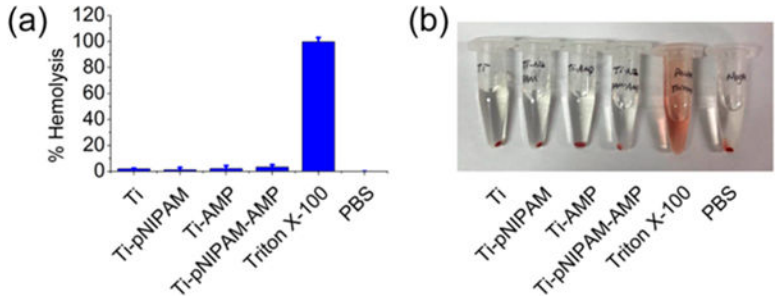

Figure 7.

Hemolysis activity of the indicated surface (a) and the corresponding photographs (b) after incubation with red blood cells for 3 h.

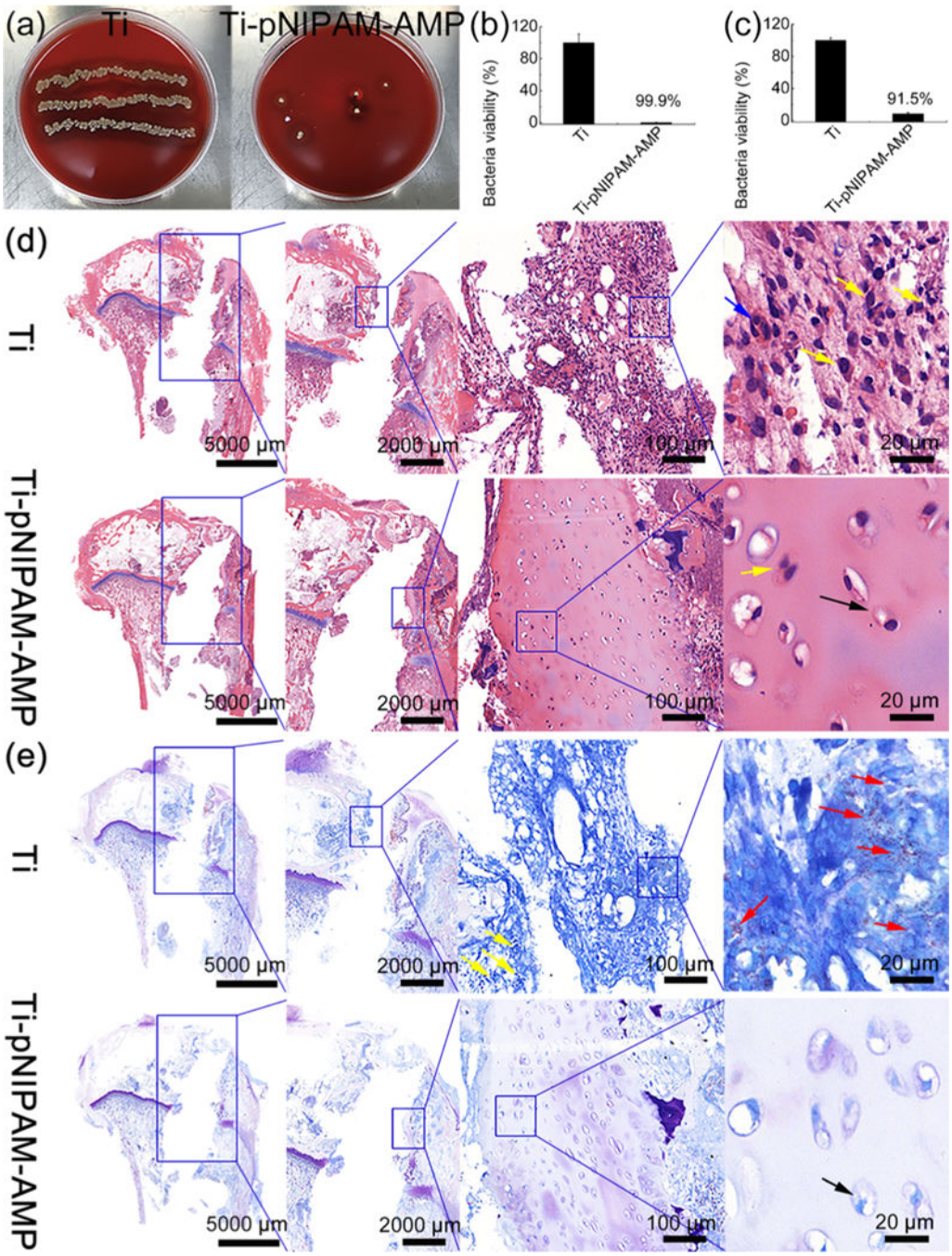

Figure 8.

In vivo characterization of antimicrobial activity and biocompatibility of samples after implanted in rabbit tibiae for 7 d. Before implantation, the samples were incubated with bacteria at RT. (a) Images of the Petri dishes showing the presence of bacteria (yellow spots) after the implanted samples (Left: Ti, Right: Ti-pNIPAM-AMP) were rolled over the blood agar. (b,c) Antimicrobial activity of the surfaces of different samples (b) and the tissues surrounding the corresponding samples (c). These data suggest that Ti-pNIPAM-AMP is more antimicrobial than Ti, leading to much fewer bacteria on both itself and its surrounding

tissues. (d,e) Histological images of H&E (d) and Giemsa (e) staining. The blue and yellow arrows denote osteoclasts and inflammatory cells, respectively. The red arrows denote the bacteria observed in the tissue. The black arrows denote the live bone cells. These data suggest that Ti-pNIPAM-AMP presented an antimicrobial activity at RT and increased biocompatibility in vivo.